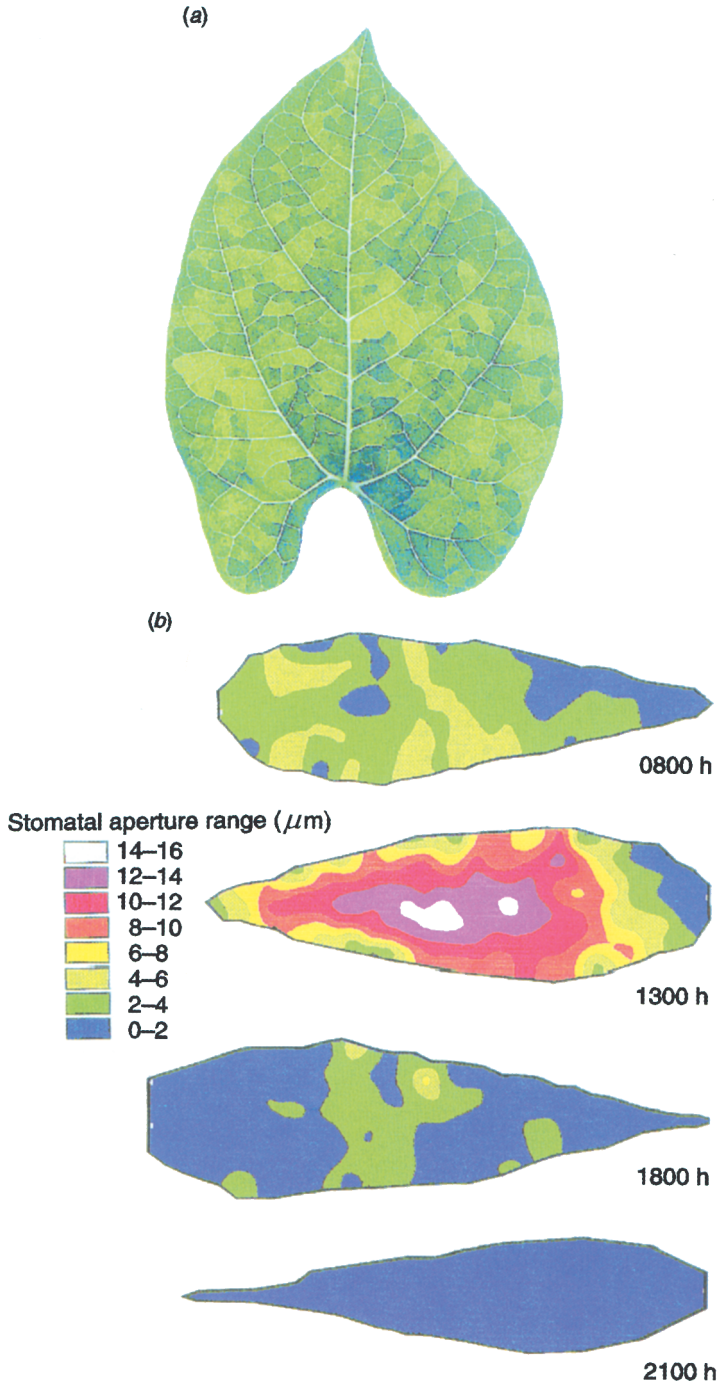
(a)
(b)
0800 h
Stomatal aperture range (μm)
14–16
12–14
10–12
8–10
6–8
4–6
2–4
0–2
1300 h
1800 h
2100 h

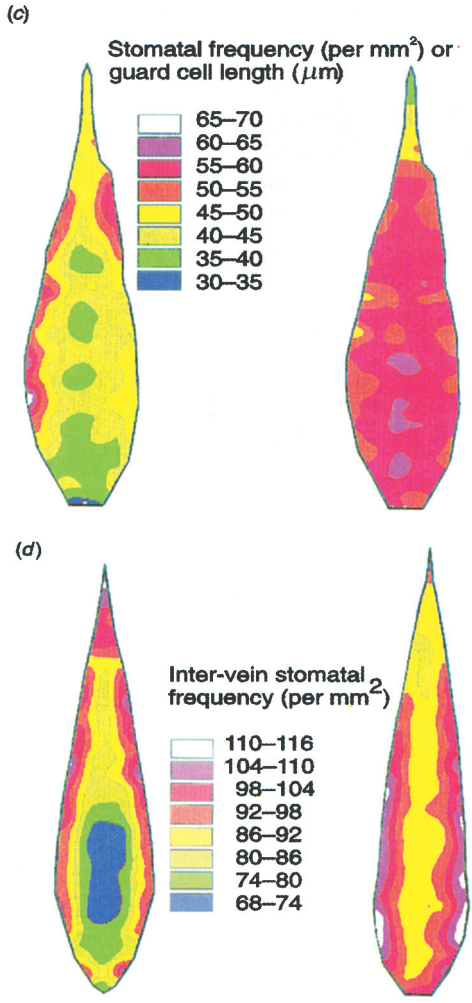

Fig. 2. Colour representations of variation in stomatal characteristics. (*a*) Patchy stomatal opening in a *Phaseolus vulgaris* leaf following excision and wilting, as visualised by vacuum infiltration (leaf length 79 mm). (*b*) Maps of mean stomatal aperture over the surface of *Commelina communis* leaves in a glasshouse at different times of day (new presentation of data of Smith *et al.*, 1989). The leaves were, in order, 90, 87, 96 and 115 mm long. (*c*) Maps of mean stomatal frequency (left) and guard cell length (right) over the surface of a *C. communis* leaf (new presentation of data of Smith *et al.*, 1989). (*d*) Maps of inter-vein stomatal frequency in fully expanded leaves from *C. communis* plants provided with continuous watering (left) or no water for 24 days (right).

A colour version of this figure is available for download from www.cambridge.org/9780521471091

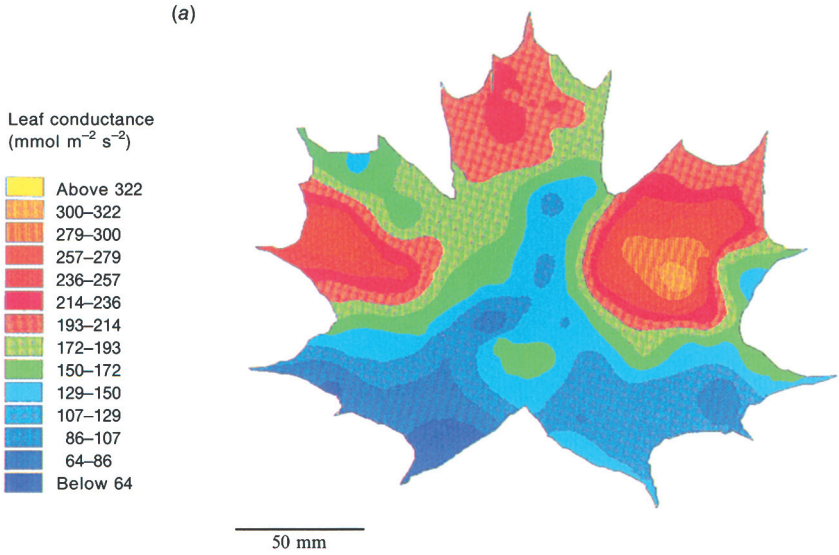

Fig. 4. Colour representations of variation in leaf conductance. (*a*) Map of leaf water vapour conductance over an *Acer pseudoplatanus* leaf in the field, based on 58 readings over about 0.8 h. Data obtained by J.D.B. Weyers and A. Yool. (*b*) Map of leaf water vapour conductance in a variegated *Ficus elastica* leaf in a glasshouse (left), based on 61 readings over about 0.3 h, and a photograph of the leaf itself (right). Data obtained by J.D.B. Weyers and A. Hunter. All data were obtained using a Mk 3 automatic porometer, Delta-T devices, Cambridge.

A colour version of this figure is available for download from www.cambridge.org/9780521471091

variable than would be expected on the basis of local variation among pores. Another striking feature of any small sample of stomata is the difference in aperture among adjacent pores (Figs. 1 and 3). For *Commelina communis*, the relative variation of stomatal apertures among adjacent pores is greater than that of other stomatal traits such as size and distance apart: Weyers & Meidner (1990) reported the respective coefficients of variation for these characteristics to be 23.0%, 7.2% and 15.4%. Spence (1987) concluded that the dispersion of stomatal aperture data (in epidermal strips) depends both on plant species and pretreatments. Laisk *et al.* (1980) noted that the frequency distributions of stomatal apertures in *Vicia faba* and *Hordeum vulgare* were symmetrical and bell-shaped, except when the mean aperture approached the extremes of zero, when the distribution was skewed right, and close to

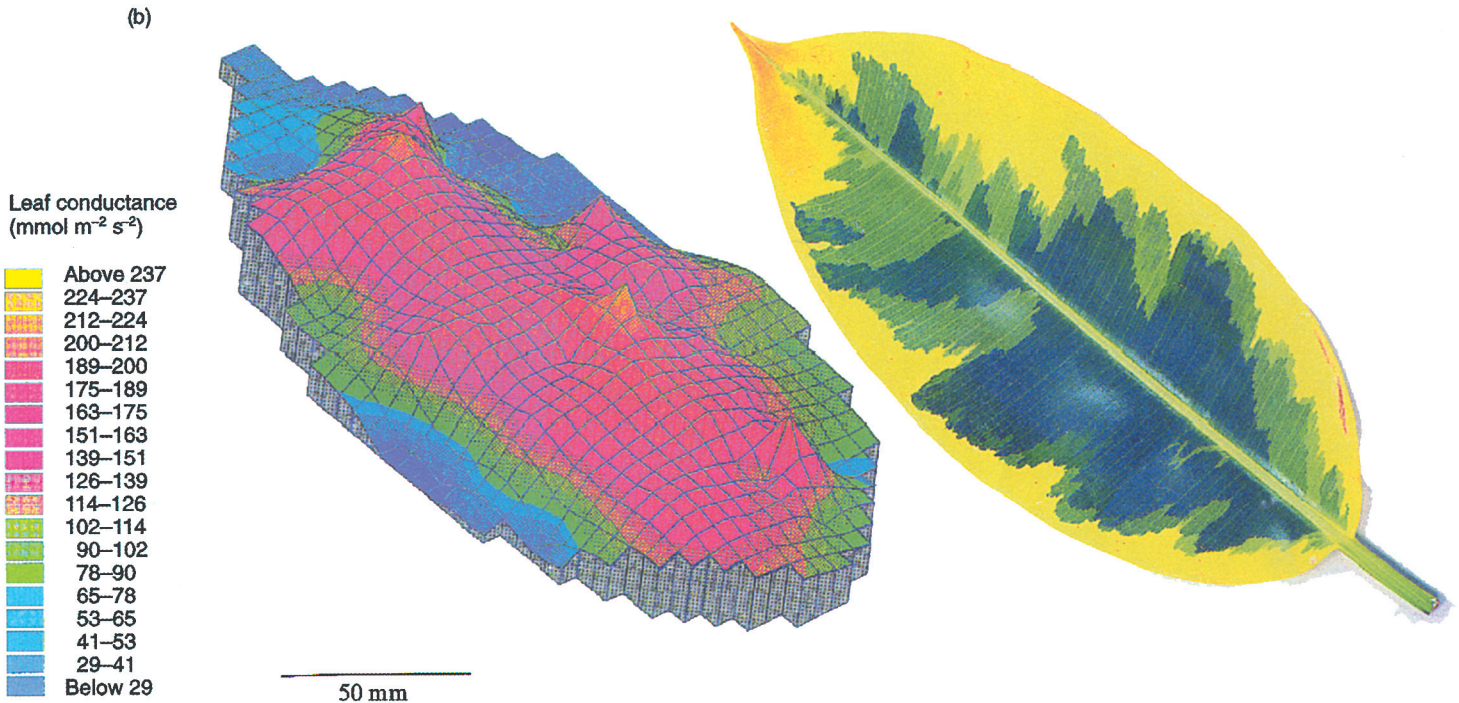
(b)
Leaf conductance
(mmol m^{-2} s^{-2})
Above 237
224–237
212–224
200–212
189–200
175–189
163–175
151–163
139–151
126–139
114–126
102–114
90–102
78–90
65–78
53–65
41–53
29–41
Below 29
50 mm

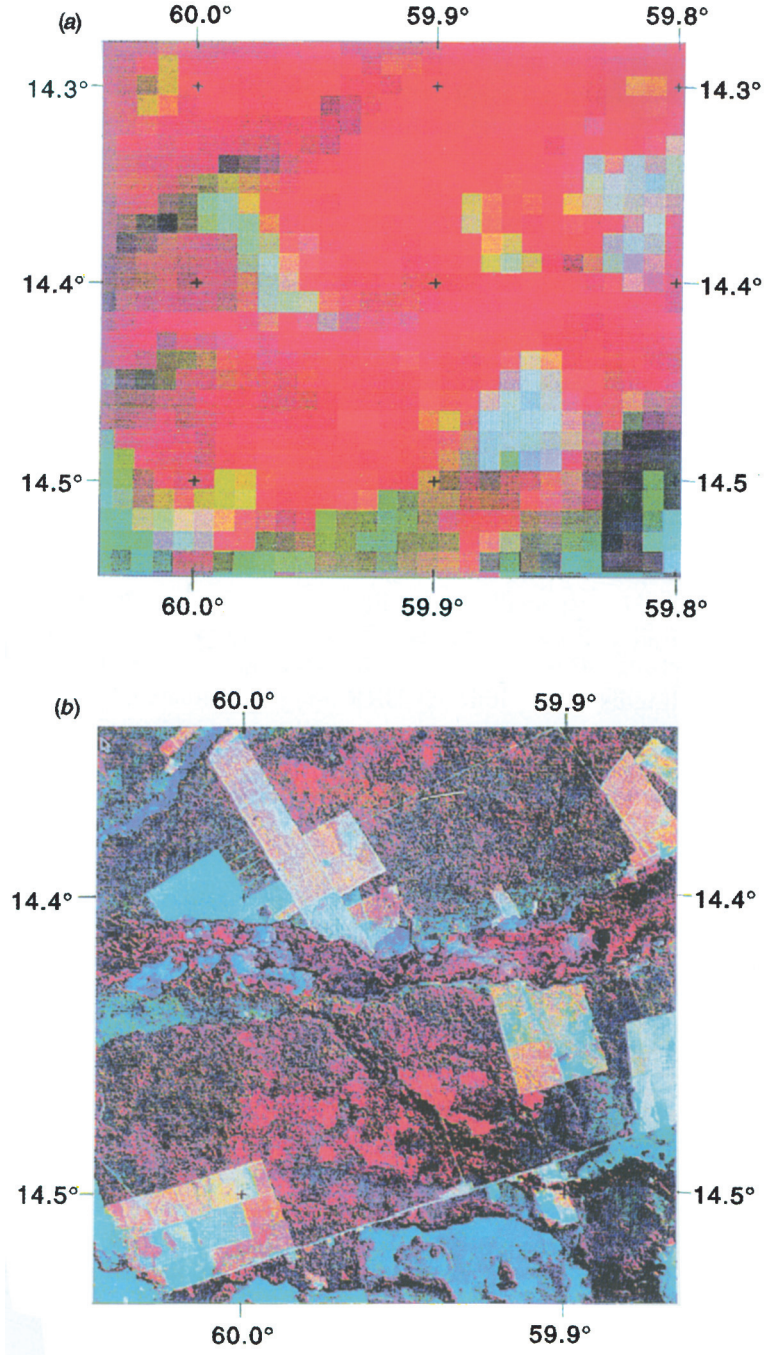

A colour version of this figure is available for download from www.cambridge.org/9780521471091

Model results and tests

GCM results

Several multiyear runs of the Colorado State University (CSU) GCM with SiB2 have now been completed. Including SiB2 increases the execution time of the GCM by about 10%, relative to that required for a simple bucket hydrology. Climate statistics indicate that the SiB2 surface parameterisation yields a realistic continental climate, and the new model runs faster and is more stable than the prior version of SiB. Details of these results are presented by Randall *et al.* (1996). It is of interest here to focus on some of the carbon cycle results. Figure 3 shows the predicted annual gross CO_2 assimilation field. The simulated total annual gross primary productivity (GPP) is 143 Gt. This value is very sensitive to the simulated climate and varies between 125 and 150 Gt per year, depending on the versionn of the GCM used. Assuming that global GPP should be 2–2.5 times net primary productivity (NPP), this value is consistent with most recent estimates of NPP.

With these results it is possible to analyse the impact of the carbon

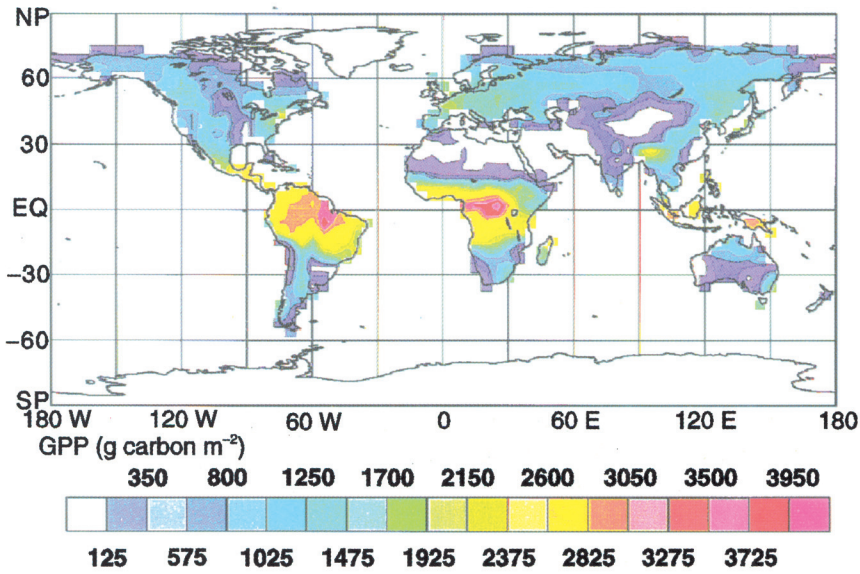

Fig. 3. A map of the distribution of annual GPP predicted by the SiB2 GCM model at a $4° \times 5°$ resolution.

A colour version of this figure is available for download from www.cambridge.org/9780521471091

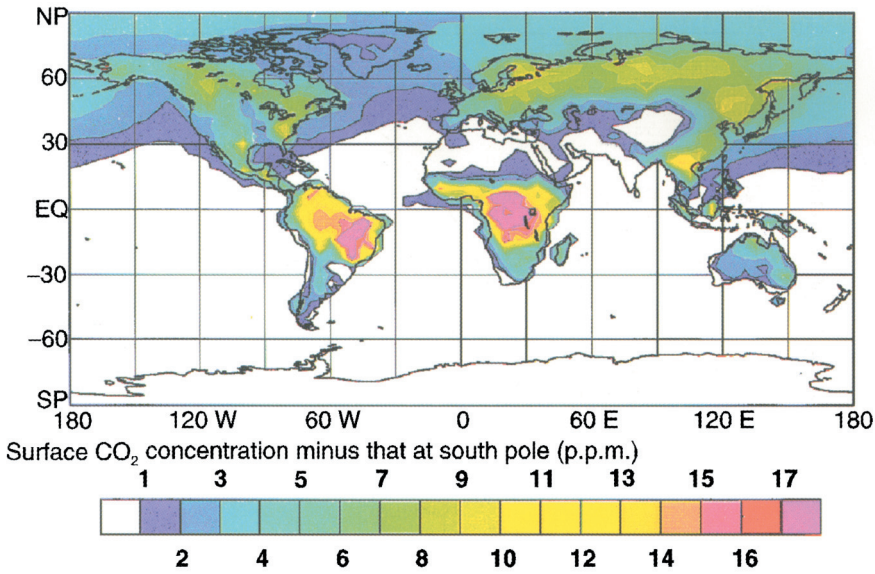

Fig. 5. Annual mean surface concentration (p.p.m.) of CO_2 simulated using SiB2 in the CSU GCM (SiB2 contribution *only*). The model was initialised with a globally uniform concentration and integrated for four years to reach equilibrium between surface fluxes and atmospheric transport. Only the effects of the annually balanced exchanges between the land surface and atmosphere are represented here. The annual net flux was close to zero at every model grid point. The concentration at the south pole has been subtracted.

A colour version of this figure is available for download from www.cambridge.org/9780521471091

integrated A_c, which was 1110 g carbon m^{-2} per year from that forested site. This is close to the simulated output from that region in the model (1260 g carbon m^{-2} per year). They observed a net seasonal accumulation of carbon (S) of 370 g carbon m^{-2} per year, and this was used to constrain our calculation of respiration in Fig. 6. No other tuning was done. The simulated seasonal pattern of A_m is close to the observed. Simulated seasonal courses of A_c, R_g and A_m for other ecosystems are plausible, but long-term CO_2 exchange measurements are not available for comparison.

Local-scale simulations

Off-line simulations using SiB2 have been conducted for comparison with daily courses of CO_2 and energy flux measurements made as part of the FIFE (first ISLSCP field experiment) (Verma, Kim & Clement,